Mechanistic Evidence of a Ni(0/II/III) Cycle for Nickel Photoredox Amide Arylation

Robert D. Bradley, Brennan D. McManus, Jessalyn G. Yam, Veronica Carta, and Ana Bahamonde*[a]

[a] R. D. Bradley, B. D. McManus, J. G. Yam, Dr. V. Carta, and Dr. A. Bahamonde
Chemistry Department, University of California, Riverside
501 Big Springs Rd., Riverside, CA 92521 (USA)
E-mail: ana.bahamonde@ucr.edu

Supporting information for this article is given via a link at the end of the document.

Abstract: This work demonstrates the dominance of a Ni(0/II/III) cycle for Ni-photoredox amide arylation, which contrasts with other Ni-photoredox C-heteroatom couplings that operate via Ni(I/III) self-sustained cycles. The kinetic data gathered when using different Ni precatalysts supports an initial Ni(0)-mediated oxidative addition into the aryl bromide. Using $NiCl_2$ as the precatalyst resulted in an observable induction period, which was found to arise from a photochemical activation event to generate Ni(0) and to be prolonged by unproductive comproportionation between the Ni(II) precatalyst and the in-situ generated Ni(0) active species. Ligand exchange after oxidative addition yields a Ni(II) aryl amido complex, which was identified as the catalyst resting state for the reaction. Stoichiometric experiments showed that oxidation of this Ni(II) aryl amido intermediate was required to yield functionalized amide products. The kinetic data presented supports a rate-limiting photochemically-mediated Ni(II/III) oxidation to enable C−N reductive elimination. An alternative Ni(I/III) self-sustained manifold was discarded based on EPR and kinetic measurements. The mechanistic insights uncovered herein will inform the community on how subtle changes in Ni-photoredox reaction conditions may impact the reaction pathway, and have enabled us to include aryl chlorides as coupling partners and to reduce the Ni loading by 20-fold without any reactivity loss.

Introduction

In recent years, the use of Ni-photoredox dual systems to promote C–heteroatom bond-forming reactions has received great interest from the chemical community.[1] These protocols are characterized by C–heteroatom reductive elimination steps under mild conditions, enabled by accessing either excited[1b, 1e, 2] or oxidized[1c, 1d, 2h, 3] Ni species. Although there have been extensive efforts made to expand the scope of Ni-photoredox-catalyzed C-heteroatom coupling, reports describing in-depth mechanistic studies of such reactions have been scarce.[2e, 3g, 4] Quantum yield measurements for both amine and alcohol arylations have uncovered Ni(I/III) self-sustained "dark cycles", where the photochemical steps served only to initiate the catalytic cycles. These studies were leveraged to design other Ni(I/III) cycles for C-heteroatom couplings in the absence of photocatalysts or light, utilizing electrochemical or chemical reductants.[4d, 4e]

In this context, our lab recently reported a Ni-photoredox-catalyzed amide arylation reaction.[5] The main advantage of this methodology is that it circumvents the high temperatures that other transition metal-mediated amide functionalization strategies require.[6] To further leverage the wider scope that milder temperatures may enable, our optimal reaction conditions avoid the need for strong alkoxide bases that are commonly used in amide functionalization reactions. This facilitated access to a large substrate scope, which included epimerizable stereocenters and, key to the results presented in this paper, also presented a rare example of a Ni-photoredox C–heteroatom cross-coupling reaction lacking a redox-active base. The central role of bases like DABCO and quinuclidine as electron shuttles facilitating electron transfers between the photocatalyst (PC) and the reaction intermediates has been highlighted by Nocera, Scholes, and MacMillan.[3g, 4c]

We were intrigued by the mechanistic impact that substituting a redox-active base for an insoluble inorganic base may have on the reaction. It should be mentioned that heterogeneous photoredox systems, although less prevalent in C–heteroatom couplings, are still ubiquitous in the literature. However, the study of biphasic photochemical reactions can be challenging, as light scattering inside the reaction flask will alter the effective photon flux. Resultingly, traditional measurements like quantum yield would not be reliable. Many reports circumvent this issue by adapting the reaction conditions into a homogeneous system for ease of study, though this can alter the mechanism being probed. Instead, we decided to study the original heterogenous conditions to better understand this widespread class of photoredox reactions.

Additionally, it was hypothesized that the lower nucleophilicity of amides may favor a new reactivity paradigm distinct from the more well-understood pathways for nucleophilic amines. As a result, the Ni-photoredox heterogeneous amide arylation reaction was chosen as the case study.[5] Specifically, the nature of the photochemical step, i.e. oxidatively-induced vs. energy transfer-mediated reductive elimination was studied (Figure 1a). Also, we aimed to elucidate whether a photochemically initiated Ni(I/III) cycle or an alternative Ni(0/II/III) cycle was predominantly operating (Figures 1b and 1c, respectively).

Herein, a series of kinetic measurements, cross-over experiments, in-situ electron paramagnetic resonance (EPR) measurements,

and characterization and reactivity studies of key reaction intermediates will be discussed. The results suggest the dominance of a Ni(0/II/III) pathway, which contrasts with other mechanistic studies for C–N bond formation.[2e, 3g, 4b-d] The intricacies with which the mechanism is studied in this work should lend insight into how subtle changes in reaction conditions and components will impact Ni-photoredox reactions. By leveraging this mechanistic understanding, we have now expanded the reaction to include aryl chlorides, as well as lowered the Ni loading from the initial 10 mol% to 0.5 mol% without compromising the reaction time or product yield.

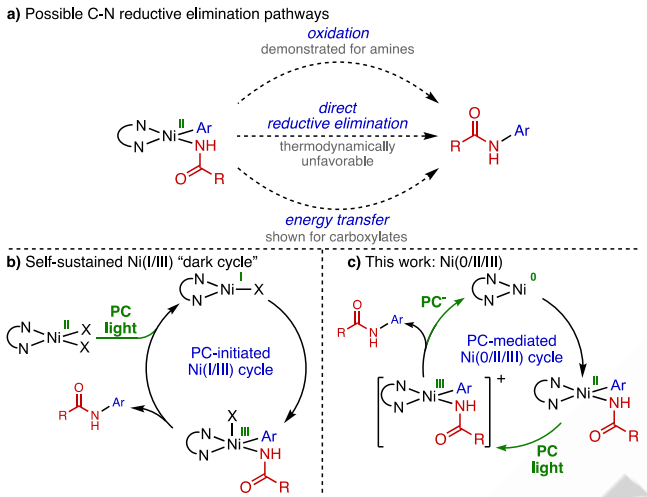

Figure 1. Transition metal-catalyzed amide arylation. (a) Possible C–N reductive elimination pathways: (b) Ni(I/III) manifold. (c) Ni(0/II/III) manifold.

Results and Discussion

Our mechanistic studies began by measuring the effect of the concentration of the different reaction components on the reaction kinetics. The reaction between 2-pyrrolidone (**1a**) and methyl 4-bromobenzoate (**2a**) with K_3PO_4 as base was chosen as a model system (Figure 2a). Key to the success of the kinetic measurements was identifying a reliable and reproducible setup that would allow us to compare multiple reactions. To do so, all the experiments were performed in identical Schlenk flasks that were positioned in pairs 1.5 cm away from the same two 427 nm Kessil lamps. In all the experiments, one of the two reactions was varied to study the effect of different conditions on the reaction rate, while the other flask was kept constant as the model conditions to ensure that the different reaction sets were comparable. Additionally, the experiments to study each reaction parameter were all performed simultaneously and utilized the same stock solutions. The stock solutions containing the Ni precatalysts and 4,4'-di-tert-butyl-2,2'-bipyridine (dtbbpy) ligand were stirred for at least 10 minutes to enable ligand exchange and dtbbpy complexation. This procedure was then conducted in duplicate on different days to ensure reproducible results.

It quickly became apparent that all reactions performed with a Ni(II) precatalyst ($NiCl_2$·glyme) displayed an induction period, with no product formation detected in the first 10-15 minutes. The presence of an induction period could be in line with either catalytic cycle, where initial reduction of the Ni(II) precatalyst to either Ni(I) or Ni(0) must occur prior to on-cycle aryl bromide oxidative addition (Figures 1b or 1c, respectively).

The photocatalyst concentration did not appear to influence the induction period or reaction rate when varied between 0.5 and 4 mol% (Figure S1). Increasing the concentration of amide and aryl bromide, with respect to the standard conditions, led to no appreciable change in either the induction period or reaction rate (Figure S2 and S3, respectively). When reducing their concentrations by one half, initial rates remained unchanged, although lower conversions were observed at longer times. Unsurprisingly, a large effect of the light intensity on the reaction rate was observed, with faster rates measured at higher light intensities (see Figure S4).

The most intriguing reaction rate changes were measured when studying the effect of different $[Ni(II)]_0$. The reaction rates for solutions containing 2.5, 5, 10, 15, and 20 mol% Ni were monitored. During these experiments, the Ni to dtbbpy ligand ratio was kept constant at 1:1.5 to reduce complexity stemming from catalyst speciation,[4d, 7] 2.5 mol% Ni reactions presented a distinct behavior from higher Ni loadings, displaying sluggish reactivity. For the rest of the reactions, a consistent trend was observed with longer induction periods measured for reactions containing a higher $[Ni(II)]_0$. After the induction periods, similar rates of product formation were observed (Figure 2a).

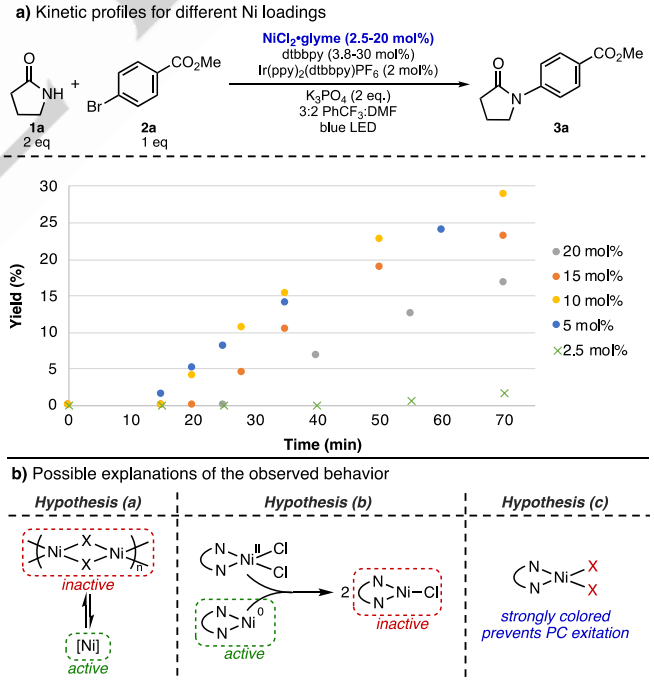

Figure 2. (a) Effect of Ni concentration on reaction rate. Reaction conditions: $NiCl_2$·glyme (0.005 mmol to 0.04 mmol), dtbbpy (0.0075 to 0.06 mmol), $Ir(ppy)_2(dtbbpy)PF_6$ (0.004 mmol), K_3PO_4 (0.4 mmol), aryl bromide **2a** (0.2 mmol), amide **1a** (0.4 mmol), 0.50 mL DMF, and 0.75 mL of $PhCF_3$. All yields were determined by ^1H NMR analysis. (b) Possible mechanistic scenarios that would align with the observed behavior.

As shown in Figure 2b, the elongation in the induction period when increasing $[Ni(II)]_0$ indicates either: (a) the formation of aggregates that sequester the Ni and are catalytically inactive, (b) the presence of bimolecular Ni processes that quench the active species, and/or (c) a possible inner filter effect where strongly colored (dtbbpy)$NiCl_2$ (or other Ni derivatives formed during the induction period) may compete with the photocatalyst for light absorption.

We first studied possibility (a), with the initial goal of assessing whether Ni aggregates are relevant to the mechanism. Aggregates would become more prevalent at higher Ni loadings. If the active catalyst species is a Ni aggregate, faster reactivity would be observed at higher Ni loadings, in stark contrast to the observed behavior (Figure 2a). If aggregates form that are catalytically inactive, the observed behavior would be expected due to the reduced effective concentration of catalytically active Ni species.

Halogen-bridged Ni(I) dimers have been postulated in analogous reactions.[4c] Resultingly, we focused on these dimers as potential aggregates that may form during the reaction. To this end, the dtbbpy Ni(I) chloride dimer was synthesized following the procedure reported by Hazari.[8] This dimer was found to be a suitable precatalyst, affording amide arylation yields comparable to those obtained with $NiCl_2$·glyme (71 vs. 72%, respectively).[5] We then measured the reaction profiles displayed when using 2.5 to 10 mol% of this dimer as the precatalyst (which equates to 5 to 20 mol% Ni loading). To mimic the $NiCl_2$·glyme reaction conditions, additional dtbbpy ligand was added to maintain the 1:1.5 Ni to ligand ratio. Under these conditions, no induction period and no effect of Ni(I) dimer loading on the reaction rate were observed, suggesting saturation kinetics with respect to Ni (Figure S6 and Figure 3c blue points). The lack of induction period when utilizing the dimer with analogous Ni loadings compared to those that displayed marked induction periods when using $NiCl_2$·glyme suggest that the formation of Ni(I) aggregates is not responsible for the induction period. Indeed, the fast kinetics and lack of an induction period observed when using the Ni(I) dimer precatalyst indicate that the dimer can readily convert to an on-cycle active species under the reaction conditions. At this stage, the formation of Ni(II) aggregates cannot be discarded as a contributor to the induction period.

We then probed the possible involvement of Ni(0) species in catalysis. The induction periods and kinetic profiles of reactions initiated with a Ni(0) precatalyst, $Ni(COD)_2$, were compared to those for reactions performed with $NiCl_2$·glyme as the precatalyst.[9] As depicted in Figure 3a and similarly to the Ni(I) dimer experiments, the reactions conducted with a Ni(0) precatalyst do not have an induction period and exhibit faster kinetics than the reactions carried out utilizing a Ni(II) source.

At this stage, it was hypothesized that if the reaction was mediated by Ni(0) (Figure 1c), the influence of $[Ni(II)]_0$ on the induction period could be due to Ni(0)/Ni(II) comproportionation events.[4d, 10] Comproportionation would be more likely at higher $[Ni(II)]_0$ and would reduce the amount of active Ni(0) catalyst, which may be required to start the reaction.

The feasibility of Ni(0)/Ni(II) comproportionation events was tested by using EPR spectroscopy to analyze a 1:1 mixture of $Ni(COD)_2$ and $NiCl_2$·glyme in $PhCF_3$. For this control experiment, a characteristic Ni(I) EPR signal was detected after 2 minutes of stirring (Figure S14). The presence of putative Ni(I) intermediates during the different catalytic reaction regimes was also studied by EPR. To test the presence of Ni(I) species in the reaction mixture during and after the induction period, reactions with 20 mol% Ni loading were sampled at 5- and 45-minute reaction times and quickly frozen with liquid N_2. No EPR signal was detected for either of the aliquots, suggesting that if Ni(I) species were indeed present, they would be present in low concentration or as the EPR silent dimer[8] (see SI for details).

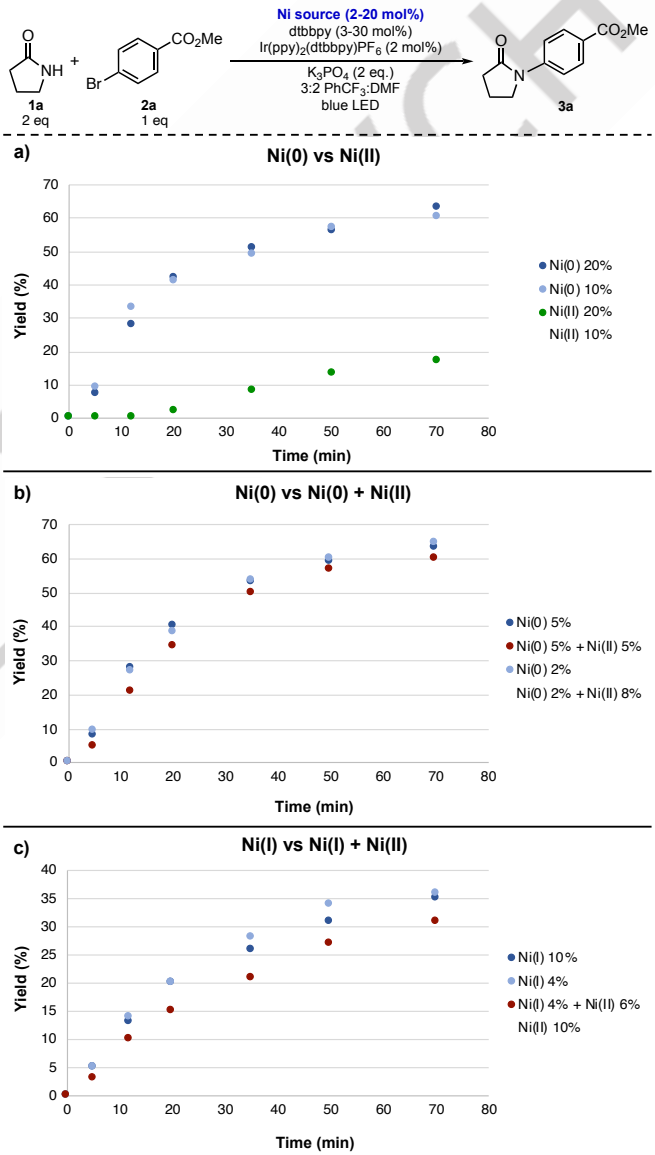

Figure 3. Effect of Ni source and loading on reaction progress. (a) Ni(0) reaction conditions: $Ni(COD)_2$ (0.004 to 0.04 mmol). (b) Ni(II) reaction conditions: $NiCl_2$·glyme (0.01 to 0.04 mmol). (c) Ni(I) reaction conditions: $(dtbbpyNiCl)_2$ (0.008 to 0.02 mmol). All reactions also contained: dtbbpy (0.006 to 0.06 mmol), $Ir(ppy)_2(dtbbpy)PF_6$ (0.004 mmol), K_3PO_4 (0.4 mmol), aryl bromide **2a** (0.2 mmol), amide **1a** (0.4 mmol), 0.50 mL DMF, and 0.75 mL of $PhCF_3$. All yields were determined by ^1H NMR analysis.

The fast kinetic profiles observed when using $Ni(COD)_2$ as the precatalyst allowed us to evaluate hypothesis (b), that bimolecular quenching forms Ni(I) complexes during the induction period, and hypothesis (c), the presence of inner filter effects at higher Ni(II) loadings. To do so, the reaction profiles for mixtures of $Ni(COD)_2$ and $NiCl_2$·glyme were compared to those containing only $Ni(COD)_2$ as the precatalyst.

First, we aimed to mimic the behavior of the initial reaction stages by comparing the reactivity of 2 mol% Ni(0) to a mixture of 2 mol% Ni(0) and 8 mol% Ni(II) (Figure 3b, lighter blue and red points, respectively). The reaction containing 2 mol% Ni(0) exhibited a profile similar to those measured for higher Ni(0) loadings (5-20 mol%, Figures 3a and 3b), while the solution containing both 2% $Ni(COD)_2$ and 8% $NiCl_2$·glyme displayed a short induction period followed by slower reactivity. The mixture of Ni(0) and Ni(II) again led to slightly lower reactivity when 5% $Ni(COD)_2$ and 5% $Ni(COD)_2$ + 5% $NiCl_2$·glyme reactions were studied (Figure 3b, darker blue and red points, respectively). To corroborate this trend, these experiments were repeated with a slight increase in the distance between the lamp and the reaction vessels, aiming to slow the overall kinetics and magnify the differences at early time points in Figure 3b. The same trends were observed, with a notably longer induction period observed for the mixture of 2% $Ni(COD)_2$ and 8% $NiCl_2$·glyme (Figure S10). Additionally, the same behavior was observed when studying mixtures of Ni(I) + Ni(II) (Figure 3c).

Another set of reactions was carried out to compare the reactivity of 10% $Ni(COD)_2$ to mixtures of 10% $Ni(COD)_2$ + 10% $NiCl_2$·glyme. In this case, no difference on the reaction profiles was observed (Figure S8). Notably, when comparing the profiles of reactions containing only $Ni(COD)_2$ as precatalyst, analogous rates were observed in each set of experiments, suggesting saturation kinetics on Ni at these loadings (2 to 20 mol%).

These results align with hypothesis (b), that unproductive comproportionation events between Ni(0) and Ni(II) are responsible for the induction periods observed under the standard reaction conditions initiated with $NiCl_2$·glyme (Figure 2a). In other words, as the Ni(II) precatalyst is reduced to Ni(0), at high Ni(II) loadings the Ni(0) is quenched via comproportionation and the active Ni(0) species is slow to build up. This is not inconsistent with the identical reaction rates observed for starting with 10 mol% $Ni(COD)_2$ vs. 10 mol% $Ni(COD)_2$ + 10 mol% $NiCl_2$·glyme. It is believed that at these higher Ni(0) loadings, little to no differences are observed due to competitive kinetics between Ni(0) undergoing aryl bromide oxidative addition and comproportionation. Considering that loadings as low as 2 mol% Ni(0) still display the same kinetic profile as 10 mol% Ni(0), if at least 1/5 of the Ni(0) can undergo oxidative addition over comproportionation, this would be consistent with the aforementioned identical reaction rates for 10 mol% Ni(0) vs. 10 mol% $Ni(COD)_2$ + 10 mol% $NiCl_2$·glyme.

In contrast to the saturation kinetics measured for Ni, a marked effect of the light intensity on the reaction rate was observed. As a result, it would be expected that the addition of species that slow the reaction due to competitive light absorption would have an increasingly negative effect with the chromophore concentration. Although Ni(II) species are highly colored, increasing the initial concentration of Ni(II) in Ni(0)/Ni(II) precatalyst mixtures from 5 to 10 mol% did not lead to a prolonged induction period (Figure S8). Thus, these results are not consistent with hypothesis (c), and the induction period cannot be due to inner filter effects.

Based on these results, it was hypothesized that the addition of a weak reductant should reduce the induction period. This was tested by comparing the kinetic profiles of the standard reaction conditions with 10 mol% $NiCl_2$·glyme as precatalyst to another identical reaction that included 50 mol% of triethylamine as an additive. The expected reduction of the induction period by adding a sacrificial electron source was observed under these conditions, and no effect on the kinetic profile after the initiation was observed (Figure S12).

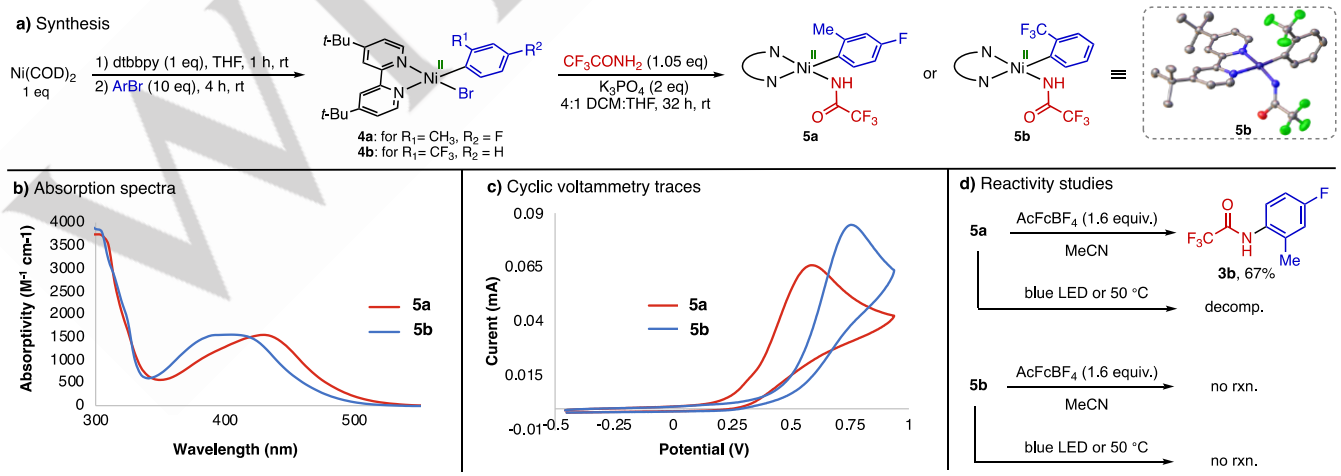

Figure 4. Synthesis, characterization, and reactivity of Ni aryl amido complexes. (a) Synthesis of **5a**, **5b**, and crystal structure of **5b**, the hydrogens have been omitted for clarity. (b) UV-Vis absorption spectra of 5 mM solutions of **5a** (red trace) and **5b** (blue trace) in CH_3CN measured in a 2 mm-path cuvette. (c) Cyclic voltammograms of 5 mM solutions of **5a** (red trace) and **5b** (blue trace) in [0.1 M] $TBAPF_6$ in CH_3CN, with 50 mV/s scan rate and glassy carbon working electrode, $Ag/AgNO_3$ reference electrode, and Pt wire auxiliary electrode. (d) Reactivity studies of the isolated complexes.

The effects of light irradiation and heat on the induction period kinetics were also tested. Together with the model reaction, an identical reaction was conducted in which the reaction flask was placed in front of the lamp but covered for the first 10 minutes of irradiation. When the progress of both reactions was compared, the induction period persisted for an additional 10 minutes for the reaction not exposed to light. Once this reaction was exposed to the incident light, the kinetics observed were parallel to the uncovered control reaction (Figure S13). This suggests that the precatalyst activation event that corresponds with the observed induction period (where the Ni(II) precatalyst is reduced to a lower-valent Ni species) requires light absorption.

To test the reactivity of a potential Ni(0) active species, we proceeded to probe the plausible steps in the catalytic cycle stoichiometrically. Aryl amido Ni complexes **5a** and **5b** were obtained by stirring the oxidative addition complex of (dtbbpy)Ni(COD) and 2-bromo-5-fluorotoluene (**4a**) or 2-bromobenzotrifluoride (**4b**) with trifluoroacetamide (**1b**) in the presence of K_3PO_4 (Figure 4a). The aryl moieties within these complexes bear an *ortho*-substituent to disfavor transmetallation and homocoupling of the Ni(II) aryl bromide (**4**) intermediates. The resulting Ni aryl amido complexes were characterized by ^1H and ^{19}F NMR spectroscopy. Additionally, a single crystal of **5b** was characterized by X-ray structural analysis, revealing a distorted square planar geometry around the Ni center.[11] Both **5a** and **5b** appeared orange in color in the solid state and in CH_3CN solutions (Figure 4b), and irreversible oxidations were observed by cyclic voltammetry ($E_{p,a}$= 0.59 and 0.75 V vs $Ag/AgNO_3$, respectively; Figure 4c). This suggests that a chemical reaction occurs following initial electrochemical oxidation of the Ni(II) aryl amido species.

To study whether the Ni(II) aryl amido intermediate is able to undergo C-N reductive elimination upon oxidation, the chemical reactivity profiles of aryl amido Ni complexes **5a** and **5b** were studied. When heated to 50 °C or irradiated at 427 nm, either no reaction or decomposition products were obtained (Figure 4d). In contrast, when **5a** was reacted with acetylferrocenium tetrafluoroborate ($E_{1/2}$ = 0.32 V vs. $Ag/AgNO_3$ in CH_3CN, Figure S16) as a chemical oxidant,[3b, 3c, 3e] arylated amide product (**3b**) was isolated in 67% yield. Air exposure also led to the formation of a trace amount of product. However, **5b** was found to be unreactive under these conditions (Figure 4d). These results are consistent with the estimated $E_{1/2}$ values from cyclic voltammetry scan rate studies for **5a** and **5b**, 0.19 and 0.50 V vs. $Ag/AgNO_3$, respectively (Figures S17-S18).[12] In comparison to the stoichiometric reactions with acetylferrocenium, the catalytic reaction between 2-bromo-5-fluorotoluene (**2b**) and trifluoroacetamide (**1b**) afforded the aryl amide product (**3b**) in lower yield (46% instead of 67% for stoichiometric). However, when 2-bromobenzotrifluoride (**2c**) was used as the aryl bromide in the catalytic reaction, no product formation was observed.

The divergent reactivity of these two complexes can be intuitively understood in terms of their relative redox potentials, with **5a** displaying a milder oxidation potential than **5b**, owing to the more electron-poor aryl ligand in the latter complex (Figure 4c). As a result, an oxidatively-induced reductive elimination will be more facile for **5a** than **5b**. Conversely, these complexes present similar absorption spectra (Figure 4b) and showed no reactivity upon irradiation, suggesting that an energy transfer-mediated mechanism is unlikely. This is in line with our prior studies that also showed no catalytic reaction occurring when a higher energy 390 nm light source was utilized in the absence of the Ir photocatalyst.[5]

Aiming to further probe the intermediacy of Ni(II) aryl amido complexes in the catalytic reaction, the suitability of **5a** as the precatalyst for the coupling of **1b** and **2a** was tested (Figure 5a). **1b** was chosen as the amide coupling partner to reduce the complexity of the reaction outcome due to the possibility of reversible amide binding. After 24 hours of irradiation, the reductive elimination product generated from Ni complex **5a** was observed in 7% yield, or 70% yield with respect to the initial 10 mol% loading of **5a**. Additionally, an excellent 91% yield was obtained for the coupling of **2a** and trifluoroacetamide **1b**, which is comparable to the yield obtained when using $NiCl_2$·glyme as the precatalyst (89%).[5] This indicates that the Ni(II) aryl amido species is a catalytically competent intermediate.

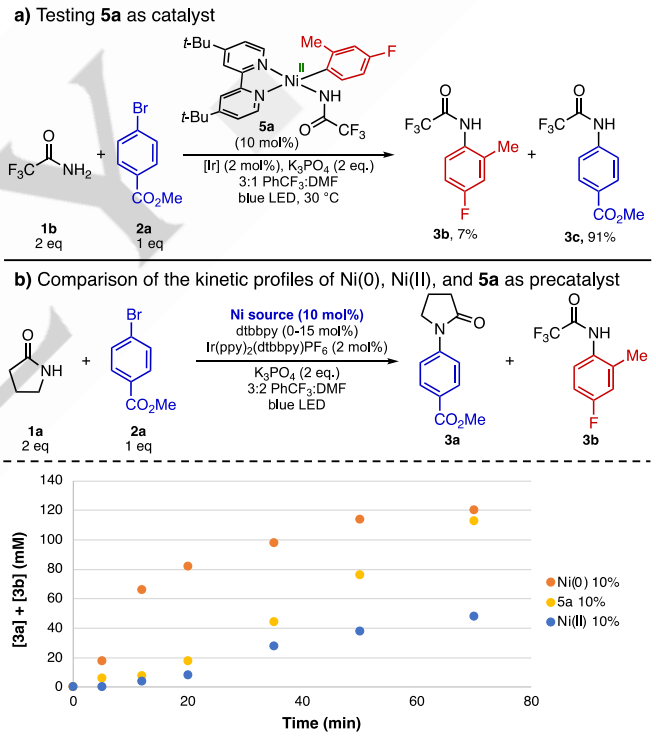

Figure 5. Probing **5a** as catalyst and reaction intermediate. (a) Testing the suitability of **5a** as catalyst for the amide functionalization. Reaction conditions: **5a** (0.03 mmol), $Ir(ppy)_2(dtbbpy)PF_6$ (0.004 mmol), K_3PO_4 (0.4 mmol), aryl bromide **2a** (0.2 mmol), amide **1b** (0.4 mmol), 0.25 mL DMF, and 0.75 mL of $PhCF_3$. All yields were determined by ^1H and ^{19}F NMR and product formation was confirmed after isolation. (b) Comparison of the reaction profiles when using Ni(0), Ni(II), or **5a** as the Ni source. Reaction conditions: for Ni(0) reaction: $Ni(COD)_2$ (0.02 mmol) and dtbbpy, (0.03 mmol). For Ni(II) reaction: $NiCl_2$·glyme (0.02) and dtbbpy, (0.03 mmol). For **5a** reaction: **5a** (0.02 mmol). All reactions also contained: $Ir(ppy)_2(dtbbpy)PF_6$ (0.004 mmol), K_3PO_4 (0.4 mmol), aryl bromide **2a** (0.2 mmol), amide **1b** (0.4 mmol), 0.50 mL DMF, and 0.75 mL of $PhCF_3$. All yields were determined by ^1H and ^{19}F NMR and the plot shows the formation of both **3a** and **3b** arylated products for a comparable yield output.

We then compared the profiles of reactions carried out using 10 mol% $Ni(COD)_2$, 10 mol% $NiCl_2$·glyme, and 10 mol% **5a** (Figure 5b). The reaction containing **5a** as catalyst showed a distinct profile compared to the other two traces. Two different regimes of slow kinetics at the beginning followed by fast kinetics were observed. During the first 10 minutes, the formation of **3b** at a slower rate was observed. Subsequently, after 10 minutes the formation of both **3b** and **3a** was detected. At this stage, the formation of **3b** remained slower than the formation of **3a**. It is hypothesized that the lower reactivity displayed when yielding **3b** is due to the steric congestion around the Ni center in complex **5a**. The *ortho*-substituted aryl group within **5a** was introduced to slow bimolecular reactions to allow for tractable synthesis and isolation, specifically to prevent the biaryl formation via transmetallation between two different complexes. It is believed that this design also slows other bimolecular processes, which in this case reduces the rate of oxidatively-induced reductive elimination. This lower reactivity is also observed under catalytic conditions, where the reaction time varies from 24 hours for **3a** to 5 days for **3b.**

Considering the kinetic data as a whole for the standard catalytic conditions, the observation of saturation behavior in all reaction components except for light suggests that oxidatively-induced reductive elimination may be the turnover limiting step, with Ni(II) aryl amido complex **5** as the catalyst resting state. To test this hypothesis, the progress of the catalytic reaction between 2-bromo-5-fluorotoluene (**2b**) and trifluoroacetamide (**1b**) was monitored by ^{19}F NMR with 10 mol% $Ni(COD)_2$ as the precatalyst. After 20 minutes of irradiation, the Ni(II) aryl amido **5a** was observed and integrated to 30% of the overall Ni loading, and, notably, no oxidative addition complex **4a** was detected.

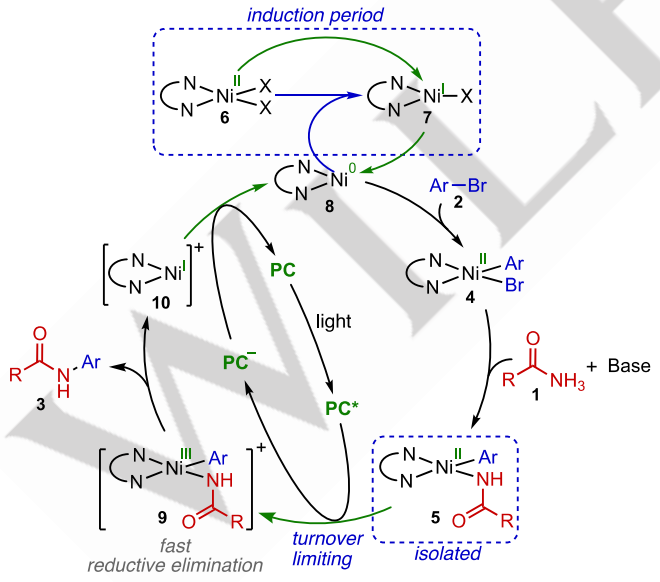

Figure 6. Proposed mechanism.

Based on the results described, Figure 6 depicts the proposed Ni(0/II/III) catalytic cycle. An induction period dependent on light intensity and Ni loading is observed when a Ni(II) precatalyst is employed (Figure 2a). The green arrows depict the light-mediated steps that facilitate the initial Ni(II) reduction (**6**→**7**→**8**). Additionally, the longer induction periods observed at higher Ni(II) loadings have been associated with Ni(0)/Ni(II) comproportionation events (blue arrows). The feasibility of this side reaction, well-precedented in the literature, has been established for this system using EPR studies.[4d, 10]

Upon formation of the Ni(0) complex, aryl halide oxidative addition to render complex **4** has been independently demonstrated to be facile. Next, in-situ ^{19}F NMR studies of the catalytic reaction progress between **1b** and **2b** showed that formation of Ni aryl amido **5** readily occurs. It should be noted that isolated oxidative addition complexes **4a** and **4b** were reacted with amide **1b** in the presence of the same inorganic base (K_3PO_4) to synthesize the amido complexes **5a** and **5b** in quantitative yields (Figure 4a). A rate-limiting photochemical oxidation is proposed to generate Ni(III) complex **9**, which can readily undergo reductive elimination as suggested by the irreversible cyclic voltammetry traces for **5** and its observed reactivity with acetylferrocenium tetrafluoroborate (Figure 4c and d). After product formation, a Ni(I) intermediate (**10**) is formed. This species, along with Ni(I) intermediate **7**, are likely in equilibrium with their halide-bridged Ni(I) dimeric forms, which was shown to be a suitable precatalyst in the case of the neutral Ni(I) dimer (Figure S6 and Figure 3c, blue points).[4c, 8] These dimer equilibria are not shown in Figure 6 for simplicity. Subsequent electron transfer from the reduced photocatalyst is proposed to regenerate Ni(0) complex **8**, allowing both catalytic cycles to resume.

An alternative pathway where **10** undergoes oxidative addition into the aryl bromide and ligand exchange to directly access Ni(III) aryl amido **9** (i.e. Ni(I/III) self-sustained cycle, Figure 1b) cannot be definitively ruled out at this stage.[3g, 4b-d] To further challenge the hypothesis that a Ni(0/II/III) cycle and not a Ni(I/III) mechanism is predominant for this reaction, the kinetic profiles were compared to profiles measured when utilizing Zn as a chemical reductant under light-free conditions (Figure 7). This approach has been shown to facilitate access to Ni(I/III) cycles in the context of alcohol, amine, and carboxylic acid arylations by the Nocera group.[4e] We initially tested the reactivity of the Zn system by

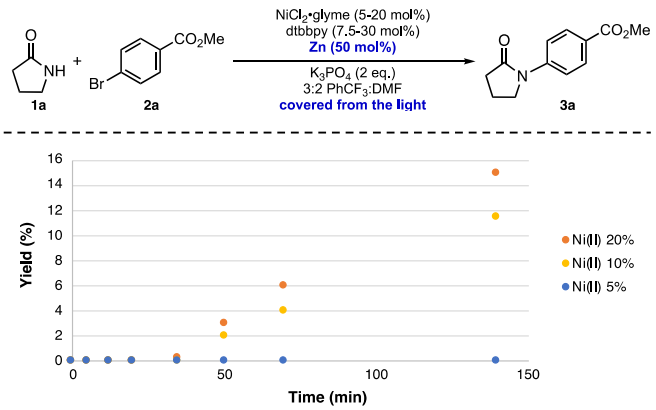

Figure 7. Effect of Ni concentration on reaction rate utilizing Zn as chemical reductant in the absence of photocatalyst and light. Reaction conditions: $NiCl_2$·glyme (0.01 mmol to 0.04 mmol), dtbbpy (0.015 to 0.06 mmol), Zn (0.1 mmol), K_3PO_4 (0.4 mmol), aryl bromide **2a** (0.2 mmol), amide **1a** (0.4 mmol), 0.50 mL DMF, and 0.75 mL of $PhCF_3$. All yields were determined by ^1H NMR analysis.

replacing the light irradiation and photocatalyst with different Zn loadings. After 24 hours of stirring at room temperature, reactions carried out with 10 mol% $NiCl_2$·glyme and 5 mol% Zn showed no reactivity, and a 39% yield of the arylated amide **3a** was obtained when utilizing 50 mol% Zn under analogous conditions.

A 50 mol% Zn loading was then chosen to study how different Ni(II) loadings affect the kinetic profiles of these transformations. As depicted in Figure 7, these unoptimized conditions generally lead to poor reactivity when compared to our photochemical conditions. Using 50 mol% Zn, an induction period is also observed, likely due to slow initial reduction of the Ni(II) precatalyst by the insoluble Zn reductant. It should be noted that the original report includes redox-active bases, which are known to accelerate these electron transfers.[4e] When comparing the effect of Ni loading on the kinetic profiles, a slight reduction of the induction period and faster kinetics are observed for higher Ni loadings. Notably, this behavior is opposite to the trend observed for the photochemical reaction under study, which presents longer induction periods for higher Ni(II) loadings and saturation kinetics in this range of Ni concentrations. These striking differences in the Ni loading effect strongly suggest that different reaction mechanisms are at play in these two systems.

Therefore, it is proposed that, if operative, a Ni(I/III) manifold likely presents a minor contribution to the mechanistic landscape in our photochemical system. Critically, in a self-sustained Ni(I/III) cycle, one would expect that the use of Ni(0)/Ni(II) mixtures (shown to generate Ni(I) in solution) would outperform reactions carried out with a Ni(0) precursor. Here, the opposite effect was observed. The only way to reconcile this behavior with a Ni(I/III) cycle would be if catalytically inactive Ni(I) aggregates are formed at high concentrations of Ni(I).[4c, 8] However, we have discarded this possibility by verifying that the Ni(I) chloride-bridged dimer is an excellent precatalyst. Moreover, no Ni(I) EPR signal was detected during the catalytic reaction, suggesting that the concentration of mononuclear Ni(I) species is low. In contrast, Ni(II) aryl amido **5a** was detected by ^{19}F NMR during the catalytic reaction.

Table 1. Leveraging mechanistic studies for further reaction optimization.[a]

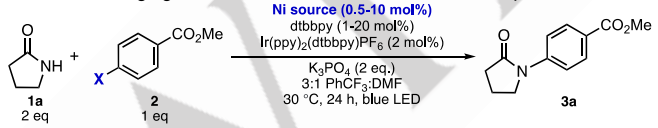

Entry	Ni source	Ni loading	Halogen (**X**)	Yield
1	$NiCl_2$·glyme	10 mol%	Br	72% [b]
2	$Ni(COD)_2$	0.5 mol%	Br	73%
3	$NiCl_2$·glyme	10 mol%	Cl	<5%
4	$Ni(COD)_2$	10 mol%	Cl	58%

[a] Reaction conditions: Ni (0.02-0.001 mmol), dtbbpy (0.04- 0.002 mmol), $Ir(dtbbpy)(ppy)_2PF_6$ (0.004 mmol), K_2CO_3 (0.4 mmol), aryl halide **2** (0.2 mmol), amide **1a** (0.4 mmol), and 1 mL of 3:1 $PhCF_3$/DMF, 30 °C, 24 h. The yields were determined by ^1H NMR with an internal standard. [b] Yield of the isolated product.

Finally, we aimed to leverage our detailed mechanistic understanding to further optimize the Ni-photoredox amide arylation protocol. In our original reaction optimization campaign, no effect on the product yield was observed when the Ni source was substituted from $NiCl_2$·glyme to $Ni(COD)_2$.[5] However, the kinetic studies detailed in this paper highlight that, unlike for Ni(II), similar kinetic profiles are observed when using lower Ni(0) loadings below 5 mol%. To leverage this information, we tested the effect on the reaction yield of lowering the Ni loading from the initial 10 mol% Ni(II) to 0.5 mol% Ni(0). As shown in Table 1, a similar yield of the arylated amide was observed despite the 20-fold decrease in catalyst loading (entries 1 and 2).

Encouraged by these results, the possibility of utilizing aryl chlorides as reaction partners with Ni(0) as precatalyst was studied. Again, a striking difference between the use of Ni(II) and Ni(0) as the precatalyst was observed, with a remarkable increase in the product yield from a trace amount to 58% (Table 1, entries 3 and 4).

Conclusion

In summary, a series of mechanistic experiments have identified an induction period dependent on Ni precatalyst and loading for our heterogeneous Ni-photoredox amide arylation protocol. These kinetic analyses, taken together with stoichiometric reactivity studies, support the dominance of a Ni(0/II/III) catalytic cycle. These findings contrast with the Ni(I/III) cycles previously proposed to be operative in related Ni-catalyzed amine arylation reactions.[3g, 4b-d] It is hypothesized that the low amide nucleophilicity and the absence of a redox-active base both play a major role in the shift of mechanism. It is anticipated that this study will aid further development of Ni-catalyzed heteroatom functionalization strategies by highlighting the precatalyst influence on the initial stages of the reaction, along with the many possible pathways that these systems can display based on small reaction condition variations. Finally, we leveraged these findings to further optimize the reaction to include more challenging substrates and to reduce the Ni loading. Further investigations of the photochemical and thermal events that facilitate the initial Ni reduction for precatalyst activation are currently ongoing.

Supporting Information

The authors have cited additional references within the Supporting Information. [12], [13], [14], [15], [16], [17], [18]

Acknowledgements

The authors thank Lingchao Zhu for his assistance with the EPR measurements. This work was supported by the NSF (CHE-2235778) and the University of California, Riverside.

Keywords: amides • nickel • photochemistry • reaction mechanisms

[1] a) J. B. Diccianni, T. Diao, *Trends Chem.* **2019**, *1*, 830-844; b) C. Zhu, H. Yue, J. Jia, M. Rueping, *Angew. Chem. Int. Ed.* **2020**, *133*, 17954-17975; c) J. A. Terrett, J. D. Cuthbertson, V. W. Shurtleff, D. W. MacMillan, *Nature* **2015**, *524*, 330-334; d) E. B. Corcoran, M. T. Pirnot, S. Lin, S. D. Dreher, D. A. DiRocco, I. W. Davies, S. L. Buchwald, D. W. MacMillan, *Science* **2016**, *353*, 279-283; e) E. R. Welin, C. Le, D. M. Arias-Rotondo, J. K. McCusker, D. W. MacMillan, *Science* **2017**, *355*, 380-385.

[2] a) D. A. Cagan, D. Bím, B. Silva, N. P. Kazmierczak, B. J. McNicholas, R. G. Hadt, *J. Am. Chem. Soc.* **2022**, *144*, 6516-6531; b) P. Ma, S. Wang, H. Chen, *ACS Catal.* **2020**, *10*, 1-6; c) J. A. Malik, A. Madani, B. u. Pieber, P. H. Seeberger, *J. Am. Chem. Soc.* **2020**, *142*, 11042-11049; d) B. J. Shields, B. Kudisch, G. D. Scholes, A. G. Doyle, *J. Am. Chem. Soc.* **2018**, *140*, 3035-3039; e) L. Tian, N. A. Till, B. Kudisch, D. W. MacMillan, G. D. Scholes, *J. Am. Chem. Soc.* **2020**, *142*, 4555-4559; f) S. I. Ting, S. Garakyaraghi, C. M. Taliaferro, B. J. Shields, G. D. Scholes, F. N. Castellano, A. G. Doyle, *J. Am. Chem. Soc.* **2020**, *142*, 5800-5810; g) L. Yang, H. H. Lu, C. H. Lai, G. Li, W. Zhang, R. Cao, F. Liu, C. Wang, J. Xiao, D. Xue, *Angew. Chem. Int. Ed.* **2020**, *59*, 12714-12719; h) C. Zhu, H. Yue, P. Nikolaienko, M. Rueping, *CCS Chemistry* **2020**, *2*, 179-190.

[3] a) R. Han, G. L. Hillhouse, *J. Am. Chem. Soc.* **1997**, *119*, 8135-8136; b) K. Koo, G. L. Hillhouse, *Organometallics* **1995**, *14*, 4421-4423; c) K. Koo, G. L. Hillhouse, *Organometallics* **1996**, *15*, 2669-2671; d) F. Le Vaillant, E. J. Reijerse, M. Leutzsch, J. Cornella, *J. Am. Chem. Soc.* **2020**, *142*, 19540-19550; e) B. L. Lin, C. R. Clough, G. L. Hillhouse, *J. Am. Chem. Soc.* **2002**, *124*, 2890-2891; f) S. Z. Tasker, T. F. Jamison, *J. Am. Chem. Soc.* **2015**, *137*, 9531-9534; g) N. A. Till, L. Tian, Z. Dong, G. D. Scholes, D. W. MacMillan, *J. Am. Chem. Soc.* **2020**, *142*, 15830-15841.

[4] a) Y. Ben-Tal, G. C. Lloyd-Jones, *J. Am. Chem. Soc.* **2022**, *144*, 15372-15382; b) C. H. Chrisman, M. Kudisch, K. O. Puffer, T. K. Stewart, Y. M. L. Lamb, C.-H. Lim, R. Escobar, P. Thordarson, J. W. Johannes, G. M. Miyake, *J. Am. Chem. Soc.* **2023**, *145*, 12293–12304; c) R. Sun, Y. Qin, S. Ruccolo, C. Schnedermann, C. Costentin, D. G. Nocera, *J. Am. Chem. Soc.* **2019**, *141*, 89-93; d) Y. Kawamata, J. C. Vantourout, D. P. Hickey, P. Bai, L. Chen, Q. Hou, W. Qiao, K. Barman, M. A. Edwards, A. F. Garrido-Castro, *J. Am. Chem. Soc.* **2019**, *141*, 6392-6402; e) R. Sun, Y. Qin, D. G. Nocera, *Angew. Chem. Int. Ed.* **2020**, *59*, 9527-9533.

[5] R. D. Bradley, A. Bahamonde, *Org. Lett.* **2022**, *24*, 7134-7139.

[6] a) I. Goldberg, *Berichte der deutschen chemischen Gesellschaft* **1906**, *39*, 1691-1692; b) A. Klapars, J. C. Antilla, X. Huang, S. L. Buchwald, *J. Am. Chem. Soc.* **2001**, *123*, 7727-7729; c) P. F. Larsson, A. Correa, M. Carril, P. O. Norrby, C. Bolm, *Angew. Chem. Int. Ed.* **2009**, *121*, 5801-5803; d) C. M. Lavoie, P. M. MacQueen, M. Stradiotto, *Chem. Eur. J.* **2016**, *22*, 18752-18755; e) R. T. McGuire, T. Lundrigan, J. W. MacMillan, K. N. Robertson, A. A. Yadav, M. Stradiotto, *Angew. Chem. Int. Ed.* **2022**, *134*, e202200352; f) E. Racine, F. Monnier, J.-P. Vors, M. Taillefer, *Org. Lett.* **2011**, *13*, 2818-2821; g) P. Ruiz-Castillo, S. L. Buchwald, *Chem. Rev.* **2016**, *116*, 12564-12649; h) W. C. Shakespeare, *Tetrahedron Lett.* **1999**, *40*, 2035-2038; i) J. Yin, S. L. Buchwald, *Org. Lett.* **2000**, *2*, 1101-1104; j) F. Diederich, P. J. Stang, *Metal-catalyzed cross-coupling reactions*, John Wiley & Sons, **2008**; k) J. F. Hartwig, *Acc. Chem. Res.* **1998**, *31*, 852-860; l) A. Ricci, *Modern amination methods*, John Wiley & Sons, **2008**; m) R. Dorel, C. P. Grugel, A. M. Haydl, *Angew. Chem. Int. Ed.* **2019**, *58*, 17118-17129.

[7] D. A. Vander Griend, D. K. Bediako, M. J. DeVries, N. A. DeJong, L. P. Heeringa, *Inorg. Chem.* **2008**, *47*, 656-662.

[8] M. Mohadjer Beromi, G. W. Brudvig, N. Hazari, H. M. Lant, B. Q. Mercado, *Angew. Chem. Int. Ed.* **2019**, *58*, 6094-6098.

[9] 10 mol% Ni(COD)2 is a competent pre-catalyst in the catalytic amide arylation reaction affording the cross coupling products in comparable yields to 10 mol% NiCl2, see SI for details.

[10] A. G. Lappin, A. McAuley, in *Advances in Inorganic Chemistry, Vol. 32*, Elsevier, **1988**, pp. 241-295.

[11] Deposition numbers 2267998 (for 5b) contain the supplementary crystallographic data for this paper. These data are provided free of charge by the joint Cambridge Crystallographic Data Centre and Fachinformationszentrum Karlsruhe Access Structures service.

[12] M. C. McCormick, K. Keijzer, A. Polavarapu, F. A. Schultz, M.-H. Baik, *J. Am. Chem. Soc.* **2014**, *136*, 8992-9000.

[13] G. Song, Q. Li, D.-Z. Nong, J. Song, G. Li, C. Wang, J. Xiao, D. Xue, *Chem. Eur. J.* **2023**, *29*, e202300458.

[14] M. Deb, S. Hazra, P. Dolui, A. J. Elias, *ACS Sustainable Chem. Eng.* **2018**, *7*, 479-486.

[15] SAINT, V8.30A, Bruker Analytical X-Ray Systems, Madison, WI, 2012.

[16] SADABS, 2.03, Bruker Analytical X-Ray Systems, Madison, WI, 2016.

[17] a) Sheldrick, G. M. *Acta Cryst.* **2008**, *A64*, 112. b) Sheldrick, G. M. *Acta Cryst.* **2015**, *A71*, 3.

[18] O. V. Dolomanov, L. J. Bourhis, R. J. Gildea, J. A. Howard, H. Puschmann, *J. Appl. Crystallogr.* **2009**, *42*, 339-341.

Entry for the Table of Contents

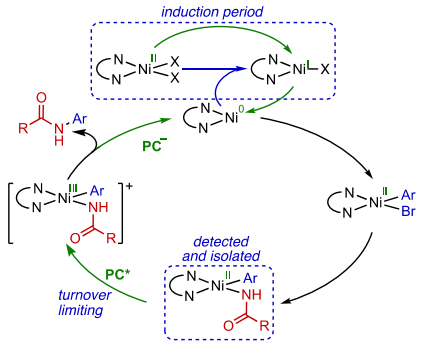

A Ni(0/II/III) cycle is uncovered for a Ni-photoredox amide arylation reaction. Identification of a precatalyst-dependent induction period, together with reactivity studies for catalytic intermediates, were key to discerning the mechanism. These findings contrast with other Ni-photoredox C−N couplings that proceed via Ni(I/III) cycles, highlighting how small changes in reaction conditions can lead to alternative pathways.

Twitter handle: @Ana_Bahamonde " Mechanistic Evidence of a Ni(0/II/III) Cycle for Nickel Photoredox Amide Arylation (Bradley and Bahamonde)"